




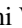












Estimation of the on-site Coulomb potential and covalent state in La_2CuO_4 by muon spin rotation and density functional theory calculations

Muhammad Redo Ramadhan ^{1,2,*} Budi Adiperdana ^{1,3} Irwan Ramli ^{1,4,†} Dita Puspita Sari ^{1,5,‡} Anita Eka Putri ^{1,2}
 Utami Widyaiswari ^{1,2,4} Harison binti Rozak ^{1,6,§} Wan Nurfadhilah Zaharim ^{1,6,||} Azwar Manaf ² Budhy Kurniawan ^{2,¶}
 Mohamed Ismail Mohamed-Ibrahim ⁶ Shukri Sulaiman ^{1,6,||} Takayuki Kawamata ^{7,#} Tadashi Adachi ⁸
 Yoji Koike ⁷ and Isao Watanabe ^{1,2,3,4,5,6,**}

¹Meson Science Laboratory, RIKEN Nishina Center, 2-1 Hirosawa, Wako, Saitama 351-0198, Japan

²Department of Physics, Universitas Indonesia, Depok 16424, Indonesia

³Department of Physics, Universitas Padjajaran, Sumedang 45363, Indonesia

⁴Department of Condensed Matter Physics, Hokkaido University, Sapporo 060-8010, Japan

⁵Department of Physics, Osaka University, Osaka 560-0043, Japan

⁶Computational Chemistry and Physics Laboratory, School of Distance Education, Universiti Sains Malaysia, Pulau Pinang 11800, Malaysia

⁷Department of Applied Physics, Tohoku University, Sendai 980-8579, Japan

⁸Department of Engineering and Applied Sciences, Sophia University, Tokyo 102-8554, Japan



(Received 3 October 2020; revised 22 March 2022; accepted 17 June 2022; published 15 July 2022)

The on-site Coulomb potential, U , and the covalent state of electronic orbitals play key roles for the Cooper pair symmetry and exotic electromagnetic properties of high- T_c superconducting cuprates. In this paper, we demonstrate a way to determine the value of U and present the whole picture of the covalent state of Cu spins in the mother system of the La-based high- T_c superconducting cuprate, La_2CuO_4 , by combining the muon spin rotation (μSR) and the density functional theory (DFT) calculation. We reveal local deformations of the CuO_6 octahedron followed by changes in Cu-spin distributions caused by the injected muon. Adjusting the DFT and μSR results, U and the minimum charge-transfer energy between the upper Hubbard band and the O $2p$ band were optimized to be 4.87(4) and 1.24(1) eV, respectively.

DOI: [10.1103/PhysRevResearch.4.033044](https://doi.org/10.1103/PhysRevResearch.4.033044)

I. INTRODUCTION

The La-based high- T_c superconducting cuprate is a typical Mott system and has a rich variety in physics, making this system still mysterious and brightly fascinating even after three decades have passed since its discovery. There are open questions on exotic electronic states that need to be investigated, like pseudogaps [1], stripes of spins and holes [2], precursor of superconducting states [3], unconventional normal states [4], and charge-ordered states [5]. These unique states are commonly realized on the basis of the strong on-site Coulomb potential, U , and covalent states of Cu $3d$ orbitals with surrounding O $2p$ orbitals [6–14]. Both properties have been suggested to be essential to describe the possible mechanism of the high- T_c superconductivity because those carry the symmetry of the wave function of the Cooper pair and electronic conducting properties [15,16].

For deeper understanding of those exotic effects caused by the on-site Coulomb potential on Cu, U , and the covalent state, the mother system of the La-based high- T_c superconducting cuprate, La_2CuO_4 (LCO), can provide an ideal playground. LCO is a typical Mott insulator and has the strong covalent state of Cu $3d$ with O $2p$ within the two-dimensional CuO_2 plane. The antiferromagnetic (AF) interaction between Cu spins leads to the formation of the AF ordered state [17–20]. The exchange coupling energy within the CuO_2 plane was suggested to be about 140 meV

*Corresponding author: redo.ramadhan@idu.ac.id; Present address: Department of Chemical Engineering, Faculty of Industrial Technology, Universitas Pembangunan Nasional “Veteran” Yogyakarta, Sleman, Yogyakarta 55283, Indonesia.

†Present address: Department of Physics, Universitas Cokroaminoto Palopo, Kota Palopo 91911, Indonesia.

‡Present address: Innovative Global Program, College of Engineering, Shibaura Institute of Technology, Saitama 337-8570, Japan.

§Joint address: USM-RIKEN Interdisciplinary Collaboration for Advanced Sciences, School of Distance Education, Universiti Sains Malaysia, 11800 Minden, Pulau Pinang, Malaysia; Present address: Graduate School of Engineering and Science, Shibaura Institute of Technology, Saitama 337-8570, Japan.

||Joint address: USM-RIKEN Interdisciplinary Collaboration for Advanced Sciences, School of Distance Education, Universiti Sains Malaysia, 11800 Minden, Pulau Pinang, Malaysia.

¶Corresponding author: budhy.kurniawan@sci.ui.ac.id.

#Present address: Department of Natural Sciences, Tokyo Denki University, Tokyo 120-8551, Japan.

**Corresponding author: nabedon@riken.jp

Published by the American Physical Society under the terms of the [Creative Commons Attribution 4.0 International license](https://creativecommons.org/licenses/by/4.0/). Further distribution of this work must maintain attribution to the author(s) and the published article's title, journal citation, and DOI.

[21]. The value of U on the Cu atom has been well investigated but still has large ambiguities of 3–10 eV [6–14], giving uncertainty on discussions of exotic electronic states of high- T_c superconducting cuprates. This is because those features contain quantum and multibody effects of electrons which are still difficult to approach either experimentally or theoretically.

Following this situation, we suggest an approach to this problem by combining the muon spin rotation (μ SR) measurement with the density functional theory (DFT) calculation including U as an adjustable parameter (DFT + U) [22–24]. The muon is a sensitive local magnetic probe and can trace the covalent state with the help of DFT + U . In this paper, we are going to show the results of this combined investigation on LCO, revealing the covalent state of Cu spins and determining U . We found three muon sites in LCO. Those muon positions were described from our DFT + U with the full view of the spatial distribution of Cu spins caused by the covalent state. Adjusting DFT + U with the μ SR results, we obtained the U value to be 4.87(4) eV followed by the determination of the minimum charge-transfer (CT) energy between the upper Hubbard band of Cu $3d_{x^2-y^2}$ and O $2p$ to be 1.24(1) eV, and the size of the magnetic moment of Cu spin to be 0.520(3) μ_B .

II. EXPERIMENTALS

A. Growth of the La_2CuO_4 single crystal

A large LCO single crystal was synthesized by the traveling-solvent floating-zone method and was confirmed to be of a single phase without impurities by using x-ray-diffraction measurement at room temperature. After oxygen reduction annealing in Ar-gas flow, the AF transition temperature, T_N , was estimated from the magnetic susceptibility measurement by using a superconducting quantum interference device (Quantum Design Co. Ltd., MPMS-XL). The crystal was sliced in parallel with the CuO_2 layer for present μ SR measurements.

B. μ SR

μ SR measurements were carried out on the GPS spectrometer at the Paul Scherrer Institut (PSI) in Switzerland by using a continuous muon source in the zero-field condition. The muon was injected into the LCO single-crystal sample keeping the initial spin polarization perpendicular to the CuO_2 plane. The time dependence of the asymmetry parameter, $A(t)$, is defined as $A(t) = \frac{F(t) - B(t)}{F(t) + B(t)}$ (μ SR time spectrum). Here, $F(t)$ and $B(t)$ are numbers of positrons counted by the forward and backward counters at t , respectively [25,26]. In order to determine internal fields at muon sites with higher accuracy, we gathered more than 6×10^8 positrons which were more than 20 times higher than usual cases.

C. DFT calculations

DFT calculations were conducted using the Vienna *Ab-Initio* Simulation Package (VASP) [27,28] with the Generalized Gradient Approximation Perdew-Wang91 (GGA-PW91) exchange-correlation functional with adjusting U between 2

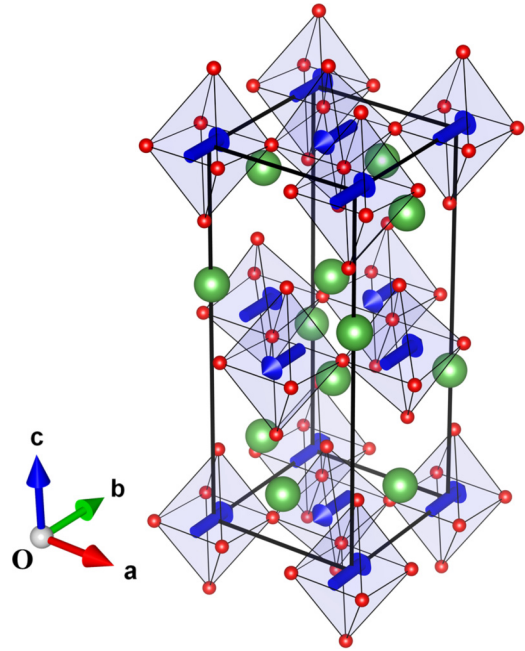


FIG. 1. Initial condition of the Cu-spin structure for the present DFT calculation study. Blue, red, and green marks are Cu spins, O, and La atoms, respectively. Cu spins form the AF spin alignment with the spin direction along to the b axis within the CuO_2 plane. This spin structure is the same as that determined from the neutron-scattering experiment [18].

and 8 eV [23,29]. The Kohn-Sham approach using the projector augmented-waves formalism was adopted as implemented in VASP [27,28]. It should be noted that DFT results generally depend on the functional [30]. Although GGA+ U is neither ideal nor the best functional to exactly describe the electronic state of LCO, this functional is well known to be valid with U in order to describe electronic states of strongly correlated systems [6,9]. Since there is no ideal full self-interaction correlated functional even now, we chose GGA+ U as the “best possible” functional for the present paper as well as other published papers [24].

The ground state of a calculation model was achieved by setting the convergence criterion of 1×10^{-4} eV. The relaxation process of all atomic positions was terminated until the magnitude of the force on each atom became less than 0.05 eV/Å following the quasi-Newton algorithm. The crystal structural symmetry was set to be orthorhombic with the $Bmab$ space group. Lattice parameters for the unit cell were set to be $a = 5.3568$ Å, $b = 5.4058$ Å, and $c = 13.1432$ Å as estimated by the neutron-scattering experiment [31].

Figure 1 indicates an initial condition of the Cu-spin structure for present DFT calculations. Cu spins form the AF alignment with the spin direction in parallel with the b axis within the CuO_2 plane. This spin structure is the same as that determined from the neutron-scattering experiment [18]. The supercell containing 32 unit cells with one muon in the formation of the $4 \times 4 \times 2$ stacking was used for all our non-collinear DFT calculations to estimate stable muon positions. RIKEN Supercomputing Facility’s HOKUSAI was used for our supercell calculations.

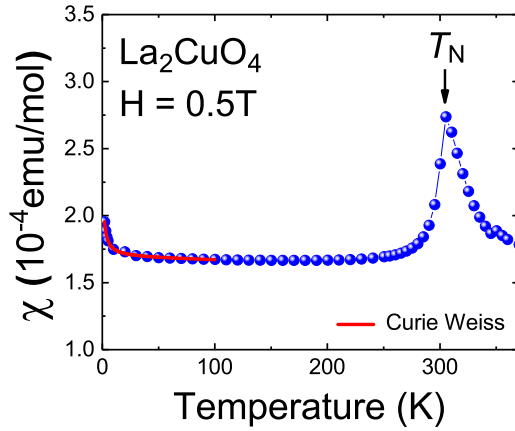


FIG. 2. Temperature dependence of the magnetic susceptibility of the La_2CuO_4 single crystal. The magnetic field of 0.5 T was applied perpendicular to the CuO_2 plane. The black arrow shows the antiferromagnetic transition temperature T_N of 309 K. The red solid line indicates the best-fit result by using the Curie-Weiss law below 100 K.

III. RESULTS

A. Characterizations of the La_2CuO_4 single crystal

Figure 2 shows the temperature dependence of the magnetic susceptibility of the LCO single crystal which was used for the present μSR study. The magnetic field of 0.5 T was applied perpendicular to the CuO_2 plane. A sharp peak was observed around 309 K which was due to the appearance of the long-range AF ordering of Cu spins [18,31]. An increase in the magnetic susceptibility was observed below about 20 K. This increase was fitted by the Curie-Weiss law. The red solid line in Fig. 2 is the best-fit result within the temperature range below 100 K. The Weiss temperature was estimated from this low-temperature analysis to be $-1.2(2)$ K. This result indicates that the increase in the magnetic susceptibility below 20 K is due to free spins which are not related to the AF ordering. Assuming that those free spins would be coming from Cu spins which appear around crystal defects, its fraction was estimated to be 0.024%.

B. μSR

Figure 3(a) shows the μSR time spectrum measured in the zero-field condition at 1.7 K on the LCO single crystal. The observation of the muon spin precession proved that Cu spins in LCO were in the AF ordered state [19]. The μSR time spectrum showed many turns of the muon spin with the slow damping rate. The muon spin precession was apparent at least up to 6 μs which was the reliable maximum measurable time. The observation of the clear muon spin recession in the long-time region indicates that the AF network of Cu spins is well coherent compared to those used in other μSR studies [19,20,32].

Figure 3(b) shows the Fourier spectrum of the muon spin precession. We confirmed three peaks. One was the main peak with a large spectral weight compared with the other two. The other two peaks were found at the higher- and lower-frequency sides with much smaller spectral weight than that of

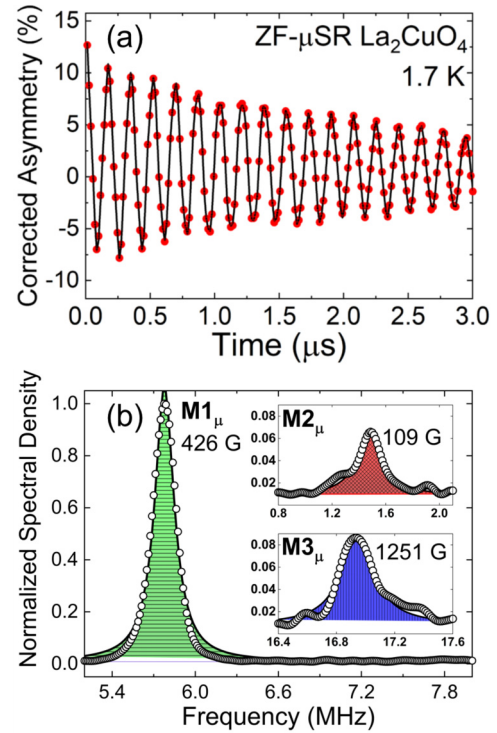


FIG. 3. (a) μSR time spectrum measured at 1.7 K on the La_2CuO_4 single crystal. The solid line is the best-fit results by using Eq. (1) with $i=1,2,3$. (b) Fourier spectrum of the muon spin precession. Solid lines show the best-fit results obtained by using the Lorentzian function. Insets show Fourier spectra of the additional two components.

the main peak. These results mean that there are three possible muon stopping positions in LCO with different occupancies. For convenience, we named the main peak, lower field, and higher field positions as $M1_\mu$, $M2_\mu$, and $M3_\mu$, respectively.

We applied the Lorentzian function to estimate the internal field at each muon site. Solid lines in Fig. 3(b) are the best-fit results for each peak. The frequency value at each peak position, ω , was converted to an internal magnetic field at the muon site, H , by the following relation:

$$\omega = \gamma_\mu H. \quad (1)$$

Here, γ_μ is the gyromagnetic ratio of μ of 135.5 MHz/T. The main peak is corresponding to the internal field of 426.7(1) G (≈ 5.78 MHz). This value is the same as that reported in the past [19]. The low-frequency one is corresponding to 109.2(4) G (≈ 1.48 MHz). This low-frequency peak was reported from the μSR study on the LCO thin film with much bigger muon-precession amplitude compared to our observed one in the bulk LCO single crystal [32]. At this moment, reasons why the amplitudes obtained in the LCO thin film and the bulk form are different are still unclear and need to be investigated. On the other hand, the high-frequency peak with the internal field of 1251.6(3) G (≈ 17.0 MHz) was not reported in the LCO thin film. There is a possibility that this high-frequency peak was not clearly observed in the LCO thin film for some reason, such as too low precession amplitude.

TABLE I. Obtained parameters from the best fit of the μ SR time spectrum by using Eq. (2) and Fourier spectra by using the Gaussian function. The ω_i was converted to the internal field at each muon site, $H_{\mu\text{SR}}^{M_i}$, following Eq. (1).

	μ SR time spectrum				Fourier spectra
	A_i (%)	$H_{\mu\text{SR}}^{M_i}$ (G)	ϕ_i (deg)	λ_i (μs^{-1})	Peak position (G)
M1 $_{\mu}$	9.228(23)	426.35(2)	-5.15(15)	0.333(20)	426.59 (1)
M2 $_{\mu}$	2.631(54)	95.9(58)	22.6(55)	5.36(26)	109.16 (39)
M3 $_{\mu}$	0.872(26)	1245.54(36)	-5.7(17)	0.50(3)	1251.55 (27)
Offset	1.879(54)	-	-	0.380(36)	-

Following this result, the time spectrum shown in Fig. 3(a) was analyzed assuming three muon sites by applying Eq. (2). Watching the time spectrum carefully, the center of the muon spin precession is shifted from the corrected zero-asymmetry position and relaxed slowly. The shift of the time spectrum from the corrected zero position was included in the analysis function as the offset component. Constant background signals which were coming from surroundings of the sample were subtracted from the time spectrum by applying this fitting method, so that the μ SR time spectrum shown in Fig. 3(a) is the background-free spectrum. The solid line in Fig. 3(a) is the best-fit result:

$$A(t) = \sum_i A_i \cos(\omega_i t + \phi_i) e^{-\lambda_i t} + A_{\text{offset}} e^{-\lambda_{\text{offset}} t}. \quad (2)$$

Here, A_i and A_{offset} , and λ_i and λ_{offset} , are initial asymmetries at $t=0$, relaxing rates of the muon spin precession and the offset component, respectively. The ω_i and ϕ_i are the frequency and phase of the muon spin precession, respectively. The ω_i is converted to the internal field at the muon site following Eq. (1). For convenience sake, we indexed the internal field at each muon site to be $H_{\mu\text{SR}}^{M_i}$ ($i=1,2,3$). The ratio among A_i is corresponding to the existing probability of the muon at each stopping site, putting $i=1,2,3$ for M1 $_{\mu}$, M2 $_{\mu}$, and M3 $_{\mu}$, respectively. All parameters obtained from the Fourier analysis and direct fitting of the time spectrum are listed in Table I.

The ratio among initial asymmetries seems to be different from that of the Fourier spectrum weight. This is due to the fast relaxation rate for M2 $_{\mu}$ compared to those for M1 and M3. After compensating the Fourier spectrum weight by the relaxation rate, both ratios became similar to each other. Accordingly, we used the ratio among initial asymmetries for simplicity to argue the population of the muon at each site.

C. DFT + U without μ

In the first attempt to combine DFT + U with the μ SR results, we tried to visualize the full view of the covalent state of Cu around the the nuclear position without the muon. Figure 4(a) exhibits the map of the Cu-spin density distribution obtained from DFT + U calculations. The U was simply set to be 5.0 eV as a convenience. The Cu-spin density on the CuO_2 plane expands from the atomic position of Cu to the in-plane O sites. This is due to the covalent state of Cu $3d_{x^2-y^2}$ with the neighboring O $2p_{\sigma}$ and causes the appearance of a partial density of Cu spin at the in-plane O position. The adjacent Cu spin also expands its density to the same in-plane O site

with the opposite sign of the spin direction and cancels the net magnetic moment at in-plane O. We found that about 18% of the Cu spin was transferred from the atomic position of Cu to in-plane O. This should be one of the reasons why the net magnetic moment of the Cu spin ($S=1/2$) is not $1 \mu_B$ but reduced to be about a half as observed by neutron-scattering experiments [18,31]. This reduction due to the covalent state explained only 36% of the total reduction in the magnetic moment of Cu, indicating that the quantum spin fluctuation effect is important to satisfy the difference [33].

In addition to this, a small amount of the asymmetric Cu-spin density was found in $2p_z$ of apical O as indicated in Fig. 4(a). The estimated amount was at most 1% of the Cu spin, and the density inside the CuO_6 octahedron is bigger than that of the outside. This result is consistent with that obtained by Lane *et al.* [13]. Consequently, the net magnetic moment at apical O is not canceled and the amount of about $0.01 \mu_B$ is left. The spin direction on apical O is opposite to that of Cu within the same CuO_6 octahedron. This small

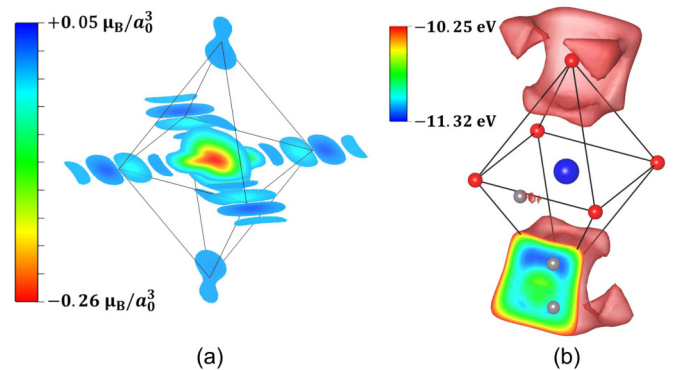


FIG. 4. (a) Three-dimensional map of the Cu-spin density in the CuO_6 octahedron of La_2CuO_4 obtained from our DFT + U calculations. The Cu-spin density expands to the in-plane O and reverses the spin direction at the other side centering the nuclear position of O as shown by the dark blue color. This means that the neighboring Cu-spin component which has the opposite spin direction as shown in Fig. 1 flows into the same in-plane O and cancels the total spin component. The a_0 in the density unit is the Bohr radius. (b) Electrostatic potential calculation results. The red area is the isosurface showing the energy level of 1.07 eV higher from the minimum potential. The energy level of the isosurface was chosen to make the position of M3 $_{\text{DFT}}$ clearly visible. Gray balls indicate three local-minimum potential positions as candidates for initial muon stopped positions.

magnetic moment at apical O cannot be ignored in the estimation of the internal field at the muon site [34].

The Cu-spin density in the vertical direction to the CuO_2 plane was also investigated by DFT in order to visualize a magnetic path along the interplane direction within the CuO_6 octahedron. However, almost no enlargement of the polarized spin-density distribution in Cu $3d_{z^2-r^2}$ was found in the preceding study [13], indicating a possibility that the interplane magnetic interaction could be driven by the direct exchange interaction between Cu $3d_{x^2-y^2}$ and $2p_z$ of apical O within the same CuO_6 octahedron. On the other hand, the angle-resolved photoelectron spectroscopy succeeded to visualize Cu $3d_{z^2-r^2}$ and a ^{139}La -NMR measurement pointed out a part of Cu-spin density was transferred to apical O via Cu $3d_{z^2-r^2}$ [35,36]. A theoretical study of low-energy Hamiltonians hypothesized active roles of Cu $3d_{z^2-r^2}$ hybridizing with O $2p_z$ [12]. These results indicate that the contribution of Cu $3d_{z^2-r^2}$ to the interplane magnetic interaction is not negligible and still an open question.

D. DFT + U with μ

As the next step, DFT + U was carried out including the muon to reproduce the μSR results. For this purpose, muon positions in LCO were investigated in advance. The precise determination of muon positions in LCO has not yet been successful in the past and was left as a long-term fundamental problem in the muon community [32,37–41].

Figure 4(b) shows our estimation of initial stopping positions of injected muons in LCO obtained from simple electrostatic potential calculations by using a unit cell since the muon has a positive charge and prefers to sit down at the minimum electrostatic potential just after it stops in the sample [40]. Three possible local minimum potential positions were found as candidates of initial muon stopping positions. We named those three positions as M1_{DFT} , M2_{DFT} , and M3_{DFT} in order to compare with the μSR results. The injected muon chooses one of those three positions to initially stop and moves to a local stable position interacting with surrounding atoms and electrons, causing local deformations of the crystal structure and electronic states in the vicinity of the muon [41,42]. There are four crystallographic equivalent sites of each muon position within the unit cell. We confirmed by using the present calculation condition including the muon that those sites were also magnetically equivalent within the calculation accuracy.

Since the number of injected muons is almost negligible compared with the number of atoms in the sample, the muon can be regarded as a superdilute magnetic impurity in DFT + U . This situation requires us to set a sufficiently large supercell structure with one muon inside in order to follow the realistic μSR experimental condition. Accordingly, the $4 \times 4 \times 2$ supercell was used for the present DFT + U including the muon. DFT calculation on a small cell with one muon is unrealistic because the number of muons is comparable to the number of unit cells of the sample in smaller cells [43]. Our modeled supercell contained 896 atoms and one muon. All atomic positions and electronic density distributions needed to be adjustable parameters within the supercell with only one muon as the magnetic impurity. This kind of supercell

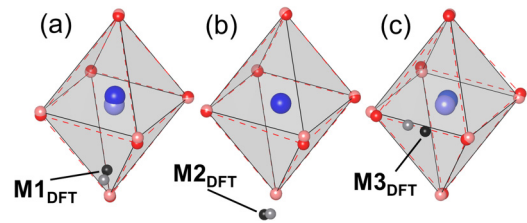


FIG. 5. Final stable muon positions for (a) M1_{DFT} , (b) M2_{DFT} , and (c) M3_{DFT} , respectively, obtained from DFT + U including the muon using the $4 \times 4 \times 2$ supercell. Gray and black balls in each panel indicate the initial and final position of the muon after the relaxation, respectively.

calculation requires larger-scale computation volume. We carried out this large-scale calculation by using the high-performance supercomputing cluster system of HOKUSAI in RIKEN.

Figures 5(a)–5(c) indicate the final muon positions and local deformations of the crystal structure estimated from our DFT + U + μ calculations. As for M1_{DFT} , the muon is located near apical O and inside the CuO_6 octahedron as demonstrated in Fig. 5(a). The muon moves further inside of the CuO_6 octahedron after relaxing its position and pushes away the Cu atom from the muon. Two in-plane O in the CuO_2 plane are pulled toward M1_{DFT} . Concerning M2_{DFT} , the muon stops near apical O as well as M1_{DFT} but outside the CuO_6 octahedron as shown in Fig. 5(b). The muon moves away a little from apical O after the relaxation and pulls one in-plane O to its side. M2_{DFT} does not affect the Cu position too much. In terms of M3_{DFT} , the muon sits in between two in-plane O and pulls them to its side and pushes away the Cu atom from the muon as exhibited in Fig. 5(c).

Those local changes in atomic positions of Cu lead to changes in the Cu-spin distribution around the muon. Figure 6 shows the results of DFT + U + μ , indicating the Cu-spin density distribution around each muon position. In the case of M1_{DFT} , the Cu-spin density becomes slightly less as shown in Fig. 6(a), resulting in the reduction of the magnetic moment of Cu overall. This reduction in the magnetic moment of Cu happens just beside the muon. The reduction ratio of the magnetic moment of Cu in the presence of the muon was

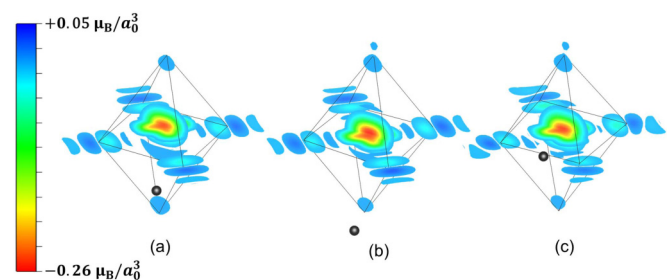


FIG. 6. Cu-spin density distribution estimated by DFT + U including the muon using the $4 \times 4 \times 2$ supercell with the muon at (a) M1_{DFT} , (b) M2_{DFT} , and (c) M3_{DFT} , respectively. Black balls in each panel indicate the final position of the muon where the muon's density has the maximum. The a_0 in the density unit is the Bohr radius.

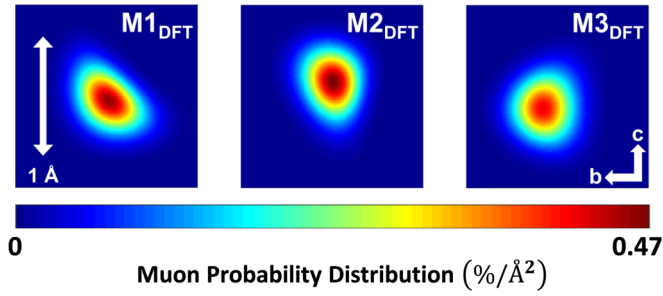


FIG. 7. Zero-point vibration motion of the muon itself around the minimum electrostatic potential for $M1_{\text{DFT}}$, $M2_{\text{DFT}}$, and $M3_{\text{DFT}}$. These are views of cross sections perpendicular to the CuO_2 plane including the local minimum potential point.

estimated to be about -5 and -1% for $M1_{\text{DFT}}$ and $M3_{\text{DFT}}$, and $\approx 0\%$ for $M2_{\text{DFT}}$.

The unbalanced spin density was also found at in-plane O which was caused by changes in the spin densities coming from the adjacent two Cu atoms. This effect was the largest for $M3_{\text{DFT}}$ as shown in Fig. 6(c) and can be qualitatively understood as follows. The balance of the Cu-spin density transferred to in-plane O is broken due to deformations of local electronic states and crystal structure which happens at one side beside the muon. This unbalanced Cu-spin density at in-plane O causes the nonzero magnetic moment. The estimated size of the additional magnetic moment was about $0.01 \mu_B$ but cannot be negligible for the estimation of the internal field at the muon site because this component appears just near the muon. Similarly, the small component of the magnetic moment at apical O slightly increased due to the change in the local Cu-spin density. All of these changes are local effects induced by the injected muon and disappear quickly beyond next neighbor unit cells.

E. Effects of the zero-point vibration motion of μ

In preceding studies, internal fields at the muon sites were always overestimated and could not explain the present μSR results even taking into account distributed Cu spins as shown in Figs. 6(a)–6(c). Accordingly, we included one quantum effect of the muon itself, which was the zero-point vibration motion [44]. This is because the muon is a fine particle with the lighter mass of about $1/9$ compared to the hydrogen and has the spatial distribution around the stopping position following the shape of the local potential. This quantum motion of the muon can be obtained by solving the Schrödinger equation around the local potential surrounding the muon as follows:

$$\left[-\frac{\hbar^2 \nabla^2}{2m_\mu} + V_\mu(r) \right] \psi_\mu(r) = E_\mu \psi_\mu(r). \quad (3)$$

Here, $V_\mu(r)$, m_μ , $\psi_\mu(r)$, and E_μ are the potential around the muon, muon's mass, wave function, and eigenvalue, respectively. The Schrödinger equation was solved numerically by using the MATLAB program.

Figure 7 shows the estimated muon spin distribution due to the zero-point vibration motion around the minimum electrostatic potential for $M1_{\text{DFT}}$, $M2_{\text{DFT}}$, and $M3_{\text{DFT}}$. These are

two-dimensional images within the cross section along the CuO_2 plane. Red- and blue-color regions indicate the high and low muon-density areas, respectively. We confirmed that more than 99% muon density is there within the $1.5\text{-}\text{\AA}^3$ cubic volume. The total sum of the dipole fields from surrounding Cu spins is calculated taking into account this muon spin density distribution.

IV. DISCUSSIONS

In order to optimize muon positions and other related parameters, the internal fields at $M1_{\text{DFT}}$, $M2_{\text{DFT}}$, and $M3_{\text{DFT}}$ were calculated on the basis of the dipole-dipole coupling, because LCO is a good insulator and the existing probability of conducting electrons around the muon is expected to be unlikely [45]. Cu-spin distributions and the muon's zero-point vibration motion were also included in the estimation of the internal field by using the following equation:

$$\sum_{i,j} \frac{1}{|\vec{r}_i - \vec{r}_j|^3} \left[3\bar{\rho}_i(\vec{r}_i - \vec{r}_j) \frac{(\vec{r}_i - \vec{r}_j)}{|\vec{r}_i - \vec{r}_j|^2} - \bar{\rho}_i \right] |\psi_j|^2. \quad (4)$$

Here, $\bar{\rho}_i$ denotes the vector data for the spin grids and $\vec{r}_i - \vec{r}_j$ denotes the relative distance between the Cu-spin-density grids with the density of ρ_i and the muon probability grids $|\psi_j|^2$. Then, we summed up all grid components obtained from our DFT calculations to estimate the internal field at the muon site. We set the radius of 50\AA centering the muon to achieve the converged results for dipole calculations. The supercell with one muon was set at the center of the calculated sphere and other areas were filled up by normal unit cells without muons.

It should be noted that multiple magnetic sites can be realized when different spin-structure domains are induced around microscopic defects in the LCO crystal as suggested from the μSR study on the LCO thin film [32]. If this is the case, those defects are expected to introduce free Cu spins as well around defects in the Cu-spin network [46,47]. Our magnetic susceptibility measurement on the LCO single crystal showed that the fraction of those kinds of free spins is very small and almost negligible. This result means that the LCO single crystal used in the present paper has less defects, indicating the uniform Cu-spin network with a single spin-structure domain.

We have already simulated internal fields at three muon sites in LCO with some different spin structures including the ones suggested from the μSR study on the LCO thin film [48]. This previous result showed that three different internal fields at our estimated three muon sites in the LCO single crystal can be quantitatively explained by one magnetic domain even though different spin states were set. Accordingly, we assumed in the present paper that one uniform magnetic spin structure which was the same as that determined from the neutron-scattering experiment appeared in the LCO single crystal [17,18], and thus the existence of three muon sites in LCO was intrinsic.

Since all muon positions, magnetic moments of Cu, and Cu-spin density distributions are related to U , the dipole-field calculation was repeated varying U from 2 to 8 eV in order to

TABLE II. Top part: Magnetic moment of the Cu spin estimated from current DFT calculations without the muon by varying U . Bottom part: Calculated internal fields at $M1_{\text{DFT}}$, $M2_{\text{DFT}}$, and $M3_{\text{DFT}}$ obtained from DFT calculations by varying U . All calculations were done with the same conditions taking into account the local deformation of the crystal structure and electronic state lead by the muon. The zero-point vibration motion of the muon was also included in the calculation.

	U (eV)												
	2	3	3.5	4	4.5	5	5.6	6	6.5	7	7.2	7.5	8
	Calculated magnetic moment without μ (μ_B)												
Magnetic moment	0.386	0.436	0.460	0.482	0.503	0.524	0.547	0.562	0.583	0.602	0.609	0.621	0.641
	Calculated internal fields, H_{DFT}^{Mi} (G)												
Muon position													
$M1_{\text{DFT}}$	336.35	376.01	384.85	391.51	429.28	446.36	450.22	471.50	474.90	491.08	503.83	507.16	523.10
$M2_{\text{DFT}}$	103.99	116.30	121.28	127.04	131.21	135.68	141.54	145.85	150.14	154.33	155.44	159.07	163.76
$M3_{\text{DFT}}$	888.06	990.60	1038.67	1077.89	1128.28	1169.74	1219.72	1241.02	1281.64	1322.98	1334.41	1364.36	1407.01

find out the optimized results. All calculated values which we have done are summarized in Table II.

Based on those results, we indexed the calculated internal fields as H_{DFT}^{Mi} ($i=1,2,3$) in order to compare with $H_{\mu\text{SR}}^{Mi}$. And then, we defined differences between both values by using the following equation:

$$\Delta H_{Mi} = (H_{\text{DFT}}^{Mi} - H_{\mu\text{SR}}^{Mi}), \quad (i = 1, 2, 3). \quad (5)$$

After this, we summed up all ΔH_{Mi} for each U with fitting-error values of internal fields, σ_i , as follows (detailed values of σ_i are listed in Table I):

$$\sum_i \frac{\Delta H_{Mi}^2}{\sigma_i^2}, \quad (i = 1, 2, 3). \quad (6)$$

Figure 8 shows the U dependence of summed up values obtained from Eq. (6). Applying the Gaussian function, U was optimized to be 4.87(4) eV. This value locates at the lower end of the U range which has been argued to be from 3 to 10 eV [6–14].

It was pointed out from theoretical studies on the Hubbard model with a square lattice that U is strongly correlated to the energy scale of the effective spin Hamiltonian which is described as $4t^2/U$ and that a border between strong and weak

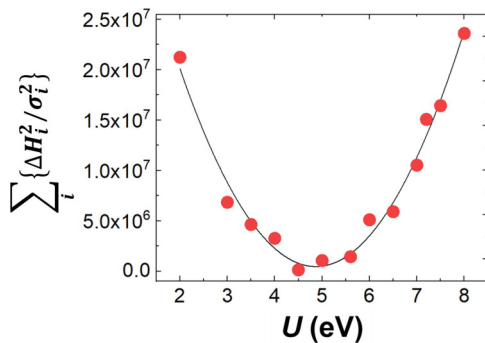


FIG. 8. Optimization of U in terms of the difference in internal fields obtained by μSR and $\text{DFT} + U + \mu$ calculations, varying U from 2 to 8 eV. The solid line is the best-fit result by using the Gaussian function. ΔH_{Mi} is the difference between $H_{\mu\text{SR}}^{Mi}$ and H_{DFT}^{Mi} ($i=1,2,3$) as described in Eq. (5). σ_i is the fitting-error value of the internal field at each $H_{\mu\text{SR}}^{Mi}$.

correlations is around $U \approx 6.5t$ [16]. Here, t is the hopping energy of electrons. Our present result of the smaller U in LCO would give limitations on discussions of t and provide possible dedicated directions to understand differences in T_c among high- T_c superconducting cuprates [49]. For instance, we suggest following the *Ab-Initio* calculation of the effective Hamiltonian that the electronic state of LCO is closer to the one-band model although more detailed comparisons with theoretical investigations are necessary [12].

Following this result of the optimization of U , the magnetic moment of Cu was estimated through the same DFT calculation processes. The optimized value was 0.520(3) μ_B in the case of LCO without the muon. The direction of the optimized Cu spin was still along the b -axis after the noncollinear refinement. The estimated magnetic moment and the spin structure were consistent with those suggested from neutron-scattering experiment [18]. In addition, optimized internal fields at each muon site in the case of $U = 4.87(4)$ eV were calculated from the dipole-field calculation using Eq. (4) to be 429.7(12), 134.1(4), and 1,147.6(35) G for $M1_{\text{DFT}}$, $M2_{\text{DFT}}$, and $M3_{\text{DFT}}$, and thus $M1_{\text{DFT}} = M1_{\mu}$, $M2_{\text{DFT}} = M2_{\mu}$, and $M3_{\text{DFT}} = M3_{\mu}$, respectively. Differences in the internal field between the μSR and $\text{DFT} + U + \mu$ were 3.4 ($\approx 1\%$), 38.2 ($\approx 40\%$), and 97.9 G ($\approx 8\%$) for $M1_{\mu}$, $M2_{\mu}$, and $M3_{\mu}$, respectively. All optimized muon positions and internal fields are summarized in Table III. Atomic positions of the CuO_6 octahedron after the optimization with the muon at $M1_{\text{DFT}}$, $M2_{\text{DFT}}$, and $M3_{\text{DFT}}$ are listed in Table IV.

Figure 9 indicates the simulated μSR time spectrum by using internal fields obtained from present $\text{DFT} + U + \mu$ calculations. We used the same values for A_i , ϕ_i , and λ_i as listed in Table I and H_{DFT}^{Mi} in order to evaluate our DFT results. The solid-red line in Fig. 9 is the simulation result. The simulated result reproduced the time spectrum fairly well, but there were still small differences between measured and simulated μSR time spectra, especially in the longer time region. This is because simulated internal fields for M1 and M3 are very close to the experimental results but the one for M2 is still fairly far. The reason why our $\text{DFT} + U + \mu$ did not perfectly reproduce the experimental result is guessed to be due to DFT's underlying principal statistical errors with regards to the pseudopotential approximation, calculation-grid resolution, cutoff energy, relaxation step for self-consistent calculation loop,

TABLE III. Cartesian components of optimized muon positions in the $4 \times 4 \times 2$ supercell and internal fields at each muon position in the style of the normalized component against the unit-cell size along the a -, b -, and c -axis. The definition of each crystal axis was the same as that used in the neutron-scattering experiment [18]. The negative signature means that internal fields direct opposite.

Muon position	Before relaxation			After relaxation			Internal fields (G)				
	a	b	c	a	b	c	Fourier	DFT	a	b	c
M1 _{DFT}	0.3839	0.5982	0.4336	0.3777	0.6175	0.4375	426.59(1)	429.7(12)	-2.81	355.06	-241.92
M2 _{DFT}	0.3928	0.5893	0.4023	0.3817	0.5968	0.3975	109.16(39)	134.1(4)	-8.54	73.89	-111.04
M3 _{DFT}	0.3660	0.5491	0.4961	0.3880	0.5502	0.4935	1251.55(27)	1147.6(35)	23.47	-1134.59	-170.17

and so on. Although the DFT + U calculation has been well established to describe electronic states of strongly correlated systems [6–14,24,42] and those statistical errors should be small, errors would be piled up during the total-energy minimization process of the nonperiodical supercell model with the muon and become nonignorable as a result in our case.

It is worthwhile to describe other value-added results obtained from the present DFT study. By using the optimized U , the band-gap structure can also be optimized, leading to the minimum CT gap between the upper Hubbard band and O $2p$ being 1.24(1) eV. This CT-gap value has been discussed within the range of 0.9–2 eV giving large ambiguity [13,50–52]. Note that our obtained value is in the ground state at 0 K. Even taking into account that the measured CT gap shows a shift for a couple of 0.1 eV to the lower-energy side with increasing temperature [52], our obtained value is fully consistent with the previous results [13,50–52]. Those facts also proved that our results revealed the realistic feature of the electronic state of LCO.

There is still one more question left for the full understanding of the μ SR results. That is how to explain differences in populations of stopped muons among the three sites. The experimental results indicate that most of the injected muons stop at M1 $_{\mu}$ as evidenced in Fig. 3(b). The ratio of populations of muons among those three sites was determined from the differences in the initial asymmetries to be M1 $_{\mu}$:M2 $_{\mu}$:M3 $_{\mu}$ =106:30:10. One possible way to address this question is to model the stopping procedure of the muon in LCO after its injection. This is left as an open question. More

DFT calculations and/or simulations will be required to tackle this problem.

V. CONCLUSION

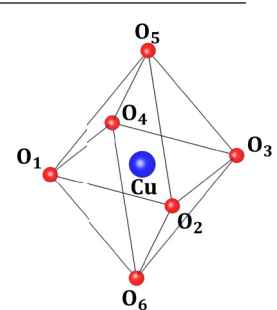
We determined the value of U , the covalent state of the Cu spin, and the CT gap energy in LCO by combining μ SR experiments and DFT calculations. Three muon positions in LCO were identified and U was precisely determined to be 4.87(4) eV, the magnetic moment of Cu was determined to be 0.520(3) μ_B , and the minimum CT gap between the upper Hubbard band and the O $2p$ band was determined to be 1.24(1) eV. The role of the perturbation introduced by the muon was found to deform the local crystal structure just around the muon, followed by subsequent changes in the surrounding electronic state in LCO. This effect leads to the slight reduction in the magnetic moment surrounding the muon.

A strong benefit of our technique is that we can achieve information of the spin structure, size of the magnetic moment, muon positions, and U in one time by analyzing one μ SR time spectrum. Especially, the U value cannot be optimized from other experimental methods with good accuracy as demonstrated in the present paper. In addition, our technique is workable for other systems on the basis of some experimental and computational conditions.

- (1) The target system has magnetic moments.
- (2) The muon spin precession should be observed.
- (3) DFT calculation is applicable.
- (4) There are accessible high-performance computing resources which can accept large-scale supercell calculations.

TABLE IV. Cartesian components of atomic positions in the $4 \times 4 \times 2$ supercell before and after the optimization of the CuO₆ octahedron with the injected muon at M1_{DFT}, M2_{DFT}, and M3_{DFT}, respectively. Each atomic position in the CuO₆ octahedron is indicated in the figure at the right end of the table. All positions are described in the style of the normalized component against the unit-cell size along the a -, b -, and c -axis. The definition of each crystal axis was the same as that used in the neutron-scattering experiment [18].

Atoms	before relaxation			after relaxation								
	without μ			with μ at M1 _{DFT}			with μ at M2 _{DFT}			with μ at M3 _{DFT}		
	a	b	c	a	b	c	a	b	c	a	b	c
Cu	0.3750	0.6250	0.5000	0.3751	0.6243	0.5087	0.3757	0.6240	0.5003	0.3739	0.6322	0.5024
O ₁	0.3125	0.5625	0.4964	0.3128	0.5635	0.4915	0.3125	0.5620	0.4942	0.3202	0.5597	0.4932
O ₂	0.4375	0.5625	0.4964	0.4369	0.5639	0.4891	0.4377	0.5622	0.4874	0.4350	0.5623	0.4929
O ₃	0.4375	0.6875	0.5036	0.4373	0.6876	0.5056	0.4381	0.6869	0.5042	0.4376	0.6898	0.5084
O ₄	0.3125	0.6875	0.5036	0.3128	0.6876	0.5059	0.3133	0.6872	0.5043	0.3102	0.6891	0.5087
O ₅	0.3750	0.6165	0.5918	0.3755	0.6112	0.5917	0.3766	0.6122	0.5918	0.3762	0.6079	0.5927
O ₆	0.3750	0.6335	0.4018	0.3742	0.6402	0.4052	0.3733	0.6408	0.4057	0.3753	0.6418	0.4076



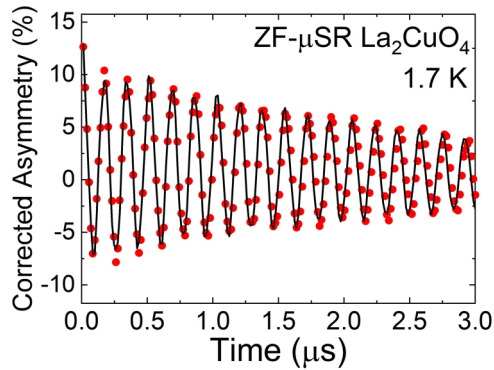


FIG. 9. ZF- μ SR time spectrum observed at 1.7 K with the simulated line by using internal fields which were estimated from the current DFT calculations. The black solid line is the trace of the simulation. The same values for A_i , ϕ_i , and λ_i listed in Table I were used, replacing $H_{\mu\text{SR}}^{\text{Mi}}$ with $H_{\text{DFT}}^{\text{Mi}}$ to draw the black solid line.

As long as those four conditions are satisfied, our developed technique to estimate U is widely applicable to any

systems. For instance, mother systems of all Cu-based high- T_c cuprates, Mott systems, heavy fermions, and strongly correlated organic molecular systems are good targets. Even using other DFT package programs like QUANTUM ESPRESSO, CASTEP, and WIEN2K, one can apply the same method described in this paper to one's own target materials. This means that the transferability of our method to other materials is quite high and widely applicable to other research fields, providing us deeper knowledge on their unique and exotic properties from a different perspective via μ SR.

ACKNOWLEDGMENTS

The authors would like to thank for technical support the muon group of PSI for carrying out the μ SR measurement and they also thank K. Ishida, A. Fujimori, and M. Ogata for valuable discussions. We would like to acknowledge the HOKUSAI supercomputing facility (Project No. G19007) of RIKEN. This work is supported by Japan Society for the Promotion of Science KAKENHI (Grants No. JP19H01841 and No. 20H04463) and International Program Associate of RIKEN.

- [1] T. Timusk and B. Statt, The the pseudogap in high-temperature superconductors: An experimental survey, *Rep. Prog. Phys.* **62**, 61 (1999).
- [2] J. M. Tranquada, B. J. Sternlieb, J. D. Axe, Y. Nakamura, and S. Uchida, Evidence for stripe correlations of spins and holes in copper oxide superconductors, *Nature (London)* **375**, 561 (1995).
- [3] Y. Wang, L. Li, and N. P. Ong, Nernst effect in high- T_c superconductors, *Phys. Rev. B* **73**, 024510 (2006).
- [4] G. S. Boebinger, Y. Ando, A. Passner, T. Kimura, M. Okuya, J. Shimoyama, K. Kishio, K. Tamasaku, N. Ichikawa, and S. Uchida, Insulator-To-Metal Crossover in the Normal State of $\text{La}_{2-x}\text{Sr}_x\text{CuO}_4$ Near Optimum Doping, *Phys. Rev. Lett.* **77**, 5417 (1996).
- [5] J. Chang, E. Blackburn, A. T. Holmes, N. B. Christensen, J. Larsen, J. Mesot, D. A. Ruixing Liang, Bonn, W. N. Hardy, A. Watenphul, M. V. Zimmermann, E. M. Forgan, and S. M. Hayden, Direct observation of competition between superconductivity and charge density wave order in $\text{YBa}_2\text{Cu}_3\text{O}_{6.67}$, *Nat. Phys.* **8**, 871 (2012).
- [6] M. T. Czyżyk and G. A. Sawatzky, Local-density functional and on-site correlations: The electronic structure of $\text{La}_{2-x}\text{Sr}_x\text{CuO}_4$ and LaCuO_3 , *Phys. Rev. B* **49**, 14211 (1994).
- [7] V. I. Anisimov, M. A. Korotin, I. A. Nekrasov, Z. V. Pchelkina, and S. Sorella, First principles electronic model for high-temperature superconductivity, *Phys. Rev. B* **66**, 100502(R) (2002).
- [8] X. Wan, T. A. Maier, and S. Y. Savrasov, Calculated magnetic exchange interactions in high-temperature superconductors, *Phys. Rev. B* **79**, 155114 (2009).
- [9] S. Pesant and M. Côté, DFT + U study of magnetic order in doped $\text{La}_{2-x}\text{Sr}_x\text{CuO}_4$ crystals, *Phys. Rev. B* **84**, 085104 (2011).
- [10] P. Werner, R. Sakuma, F. Nilsson, and F. Aryasetiawan, Dynamical screening in $\text{La}_{2-x}\text{Sr}_x\text{CuO}_4$, *Phys. Rev. B* **91**, 125142 (2015).
- [11] S. W. Jang, A. Hirofumi, H. Kino, T. Kotani, K. Kuroki, and M. J. Han, Direct theoretical evidence for weaker correlations in electron-doped and Hg-based hole-doped cuprates, *Sci. Rep.* **6**, 33397 (2016).
- [12] M. Hirayama, Y. Yamaji, T. Misawa, and M. Imada, Ab initio effective Hamiltonians for cuprate superconductors, *Phys. Rev. B* **98**, 134501 (2018).
- [13] C. Lane, J. W. Furness, I. G. Buda, Y. Zhang, R. S. Markiewicz, B. Barbiellini, J. Sun, and A. Bansil, Antiferromagnetic ground state of La_2CuO_4 : A parameter-free *ab initio* description, *Phys. Rev. B* **98**, 125140 (2018).
- [14] F. Nilsson, K. Karlsson, and F. Aryasetiawan, Dynamically screened Coulomb interaction in the parent compounds of hole-doped cuprates: Trends and exceptions, *Phys. Rev. B* **99**, 075135 (2019).
- [15] F. C. Zhang and T. M. Rice, Effective Hamiltonian for superconducting Cu oxides, *Phys. Rev. B* **37**, 3759(R) (1988).
- [16] M. Yokoyama, H. Ogata and Y. Tanaka, Mott transitions and d -wave superconductivity in half-filled-band Hubbard model on square lattice with geometric frustration, *J. Phys. Soc. Jpn.* **75**, 114706 (2006).
- [17] J. I. Budnick, A. Golnik, C. Niedermayer, E. Recknagel, M. Rossmanith, A. Weidinger, B. Chamberland, M. Filipkowski, and D. P. Yang, Observation of magnetic ordering in $\text{La}_{2-x}\text{Sr}_x\text{CuO}_4$ by muon spin spectroscopy, *Phys. Lett. A* **124**, 103 (1987).
- [18] D. Vaknin, S. K. Sinha, D. E. Moncton, D. C. Johnston, J. M. Newsam, C. R. Safinya, and H. E. King, Antiferromagnetism in $\text{La}_2\text{CuO}_{4-y}$, *Phys. Rev. Lett.* **58**, 2802 (1987).
- [19] Y. J. Uemura, Muon spin relaxation studies on T_c superconductors and related antiferromagnet, *J. Appl. Phys.* **64**, 6087 (1988).
- [20] F. Borsa, P. Carretta, J. H. Cho, F. C. Chou, Q. Hu, D. C. Johnston, A. Lascialfari, D. R. Torgeson, R. J. Gooding, N. M. Salem, and K. J. E. Vos, Staggered magnetization in $\text{La}_{2-x}\text{Sr}_x\text{CuO}_4$ from ^{139}La -NQR and μ : Effects of Sr doping in the range $0 \leq x \leq 0.02$, *Phys. Rev. B* **52**, 7334 (1995).
- [21] R. Coldea, S. M. Hayden, G. Aeppli, T. G. Perring, C. D. Frost, T. E. Mason, S.-W. Cheong, and Z. Fisk, Spin Waves and

- Electronic Interactions in La_2CuO_4 , *Phys. Rev. Lett.* **86**, 5377 (2001).
- [22] V. I. Anisimov, J. Zaanen, and O. K. Andersen, Band theory and Mott insulators: Hubbard U instead of stoner I , *Phys. Rev. B* **44**, 943 (1991).
- [23] S. L. Dudarev, G. A. Botton, S. Y. Savrasov, C. J. Humphreys, and A. P. Sutton, Electron-energy-loss spectra and the structural stability of nickel oxide: An LSDA + U study, *Phys. Rev. B* **57**, 1505 (1998).
- [24] J. Varignon, M. Bibes, and A. Zunger, Origin of band gaps in $3d$ perovskite oxides, *Nat. Commun.* **10**, 1658 (2019).
- [25] R. S. Hayano, Y. J. Uemura, J. Imazato, N. Nishida, T. Yamazaki, and R. Kubo, Zero- and low-field spin relaxation studied by positive muons, *Phys. Rev. B* **20**, 850 (1979).
- [26] Y. J. Uemura, T. Yamazaki, D. R. Harshman, M. Senba, and E. J. Ansaldo, Muon-spin relaxation in AuFe and CuMn spin glasses, *Phys. Rev. B* **31**, 546 (1985).
- [27] G. Kresse and J. Furthmüller, Efficiency of ab-initio total energy calculations for metals and semiconductors using a plane-wave basis set, *Comput. Mater. Sci.* **6**, 15 (1996).
- [28] G. Kresse and J. Furthmüller, Efficient iterative schemes for ab-initio total-energy calculations using a plane-wave basis set, *Phys. Rev. B* **54**, 11169 (1996).
- [29] J. P. Perdew, J. A. Chevary, S. H. Vosko, K. A. Jackson, M. R. Pederson, D. J. Singh, and C. Fiolhais, Atoms, molecules, solids, and surfaces: Applications of the generalized gradient approximation for exchange and correlation, *Phys. Rev. B* **46**, 6671 (1992).
- [30] J. Kulik and N. Marzari, A self-consistent Hubbard U density-functional theory approach to the addition-elimination reactions of hydrocarbons on bare FeO^+ , *Chem. Phys.* **129**, 134314 (2008).
- [31] M. Reehuis, C. Ulrich, K. Prokeš, A. Gozar, G. Blumberg, S. Komiyama, Y. Ando, P. Pattison, and B. Keimer, Crystal structure and high-field magnetism of La_2CuO_4 , *Phys. Rev. B* **73**, 144513 (2006).
- [32] E. Stülp, A. Suter, T. Prokscha, E. Morenzoni, H. Keller, B. M. Wojek, H. Luetkens, A. Gozar, G. Logvenov, and I. Božović, Magnetic phase diagram of low-doped $\text{La}_{2-x}\text{Sr}_x\text{CuO}_4$ thin films studied by low-energy muon-spin rotation, *Phys. Rev. B* **88**, 064419 (2013).
- [33] K. M. Kojima, Y. Fudamoto, M. Larkin, G. M. Luke, J. Merrin, B. Nachumi, Y. J. Uemura, N. Motoyama, H. Eisaki, S. Uchida, K. Yamada, Y. Endoh, S. Hosoya, B. J. Sternlieb, and G. Shirane, Reduction of Ordered Moment and Néel Temperature of Quasi-One-Dimensional Antiferromagnets Sr_2CuO_3 and Ca_2CuO_3 , *Phys. Rev. Lett.* **78**, 1787 (1997).
- [34] M. Miyazaki, R. Kadono, K. H. Satoh, M. Hiraishi, S. Takeshita, A. Koda, A. Yamamoto, and H. Takagi, Magnetic ground state of pyrochlore oxides close to metal-insulator boundary probed by muon spin rotation, *Phys. Rev. B* **82**, 094413 (2010).
- [35] C. E. Matt, D. Suter, and J. Chang, Direct observation of orbital hybridization in a cuprate superconductor, *Nat. Commun.* **9**, 972 (2018).
- [36] I. Watanabe, ^{139}La -NQR study of the magnetic properties of $\text{La}_{2-x}\text{M}_x\text{CuO}_4$ ($M = \text{Ba}, \text{Sr}$) for $0 \leq x \leq 0.08$, *J. Phys. Soc. Jpn.* **63**, 1560 (1994).
- [37] B. Hitti, P. Birrer, K. Fischer, F. N. Gygax, E. Lippelt, H. Maletta, A. Schenk, and M. Weber, Study of La_2CuO_4 and related compounds by μSR , *Hyperfine Interact.* **63**, 287 (1991).
- [38] E. Torikai, K. Nagamine, H. Kitazawa, I. Tanaka, S. B. Kojima, Sulaiman, S. Srinivas, and T. P. Das, Behavior of positive muons in high T_c superconductors $\text{La}_{2-x}\text{Sr}_x\text{CuO}_4$, *Hyperfine Interact.* **79**, 921 (1993).
- [39] S. B. Sulaiman, N. Sahoo, S. Srinivas, F. Hagelberg, T. P. Das, E. Torikai, and K. Nagamine, Theory of location and associated hyperfine properties of the positive muon in La_2CuO_4 , *Hyperfine Interact.* **84**, 87 (1994).
- [40] B. Adiperdana, I. A. Dharmawan, S. E. Siregar, I. Watanabe, K. Ohishi, Y. Ishii, T. Suzuki, T. Kawamata, R. Scheuermann, K. Sedlak, Y. Tomioka, T. Waki, Y. Tabata, and H. Nakamura, Muon sites estimation in La_2CuO_4 and a new vanadium cluster compound, $\text{V}_4\text{S}_9\text{Br}_4$, using electronic and nuclear dipole field calculations, *Phys. Procedia* **30**, 109 (2012).
- [41] H. U. Suter, E. P. Sroll, and P. F. Meier, Muon sites and hyperfine fields in La_2CuO_4 , *Phys. B: Condens. Matter* **326**, 329 (2003).
- [42] J. S. Möller, P. Bonfà, D. Ceresoli, S. J. Bernardini, F. Blundell, T. Lancaster, R. De Renzi, N. Marzari, I. Watanabe, and S. B. Sulaiman, Playing quantum hide-and-seek with the muon: Localizing muon stopping sites, *Phys. Scr.* **88**, 068510 (2013).
- [43] M. R. Ramadhan, I. Ramli, M. D. Umar, S. Winarsih, D. P. Sari, A. Manaf, B. Kurniawan, M. I. Mohamed-Ibrahim, S. Sulaiman, and I. Watanabe, Effect of the supercell's size on muon positions calculations of La_2CuO_4 , *Mater. Sci. Forum* **966**, 465 (2019).
- [44] F. Bernardini, P. Bonfà, S. Massidda, and R. De Renzi, Ab initio strategy for muon site assignment in wide band gap fluorides, *Phys. Rev. B* **87**, 115148 (2013).
- [45] The contact field at the muon position estimated by VASP was less than 1 G indicating that the Cu-spin density at the muon position is nearly negligible.
- [46] K. Kojima, A. Keren, G. M. Luke, B. Nachumi, W. D. Wu, Y. J. Uemura, M. Azuma, and M. Takano, Magnetic Behavior of the 2-Leg and 3-Leg Spin Ladder Cuprates $\text{Sr}_{n-1}\text{Cu}_{n+1}\text{O}_{2n}$, *Phys. Rev. Lett.* **74**, 2812 (1995).
- [47] T. Adachi, N. Oki, Risdiana, S. Yairi, Y. Koike, and I. Watanabe, Effects of Zn and Ni substitution on the Cu spin dynamics and superconductivity in $\text{La}_{2-x}\text{Sr}_x\text{Cu}_{1-y}(\text{Zn}, \text{Ni})_y\text{O}_4$ ($x=0.15-0.20$): Muon spin relaxation and magnetic susceptibility study, *Phys. Rev. B* **78**, 134515 (2008).
- [48] M. R. Ramadhan, I. Ramli, D. P. Sari, B. Kurniawan, A. Manaf, M. I. Mohamed-Ibrahim, S. Sulaiman, and I. Watanabe, Spin alignment studies on the muon-site determination in La_2CuO_4 , *Key Eng. Mater.* **860**, 154 (2020).
- [49] A. Andrade, T. Krikun, K. Schalm, and J. Zaanen, Doping the holographic Mott insulator, *Nat. Phys.* **14**, 1049 (2018).
- [50] Y. Tokura, S. Koshihara, T. Arima, H. Takagi, S. Ishibashi, T. Ido, and S. Uchida, Cu-O network dependence of optical charge-transfer gaps and spin-pair excitations in single-CuO₂-layer compounds, *Phys. Rev. B* **41**, 11657 (1990).
- [51] S. Uchida, T. Ido, H. Takagi, T. Arima, Y. Tokura, and S. Tajima, Optical spectra of $\text{La}_{2-x}\text{Sr}_x\text{CuO}_4$: Effect of carrier doping on the electronic structure of the CuO_2 plane, *Phys. Rev. B* **43**, 7942 (1991).
- [52] S. Ono, S. Komiyama, and Y. Ando, Strong charge fluctuations manifested in the high-temperature Hall coefficient of high- T_c cuprates, *Phys. Rev. B* **75**, 024515 (2007).